JOURNAL OF THEORETICAL AND APPLIED MECHANICS
46, 4, pp. 829-844, Warsaw 2008

ANALYSIS OF COUPLING MECHANISM IN LATERAL/TORSIONAL ROTOR VIBRATIONS

Zdzisław Gosiewski

Aviation Institute, Warsaw, Poland
e-mail: gosiewski@post.pl

Coupling phenomena of lateral-torsional vibrations in rotating machinery can lead to rotor unstable behaviour. In some types of rotating machinery, the angular speed is subjected to wide ranges of change. The problem is to find the range of angular speeds for which a machine exhibits stable behaviour in the presence of the coupling of dynamical modes. Usually, unstable regions are in the vicinity of angular speeds where maps of natural frequencies for both dynamical systems intersect with each other. Using the root locus method, it is described which intersections lead to unstable vibrations and why.

Key words: rotor, coupled vibrations, stability, root locus

1. Introduction

Two dynamical systems influence each other, if connected. In the case of rotating machinery, lateral and torsional vibrations are usually analysed separately. Such analysis is allowed in the case when the coupling effect is weak. When the coupling is strong, one should analyse coupled vibrations (Gosiewski and Muszyńska, 1992; Sawicki *et al.*, 2004). It appears that in the case of lightly damped structures, there are ranges of unstable rotor speeds. The unstable speed ranges are at frequencies for which the natural frequencies of both dynamical systems intersect with each other on the Campbell diagram. As far as the author knows, the literature does not contain clear explanation of the rotor instability at the intersections on natural frequencies maps.

In the paper, the coupling effect is analysed in the case of a simple three-mode rotor model (Jeffcott's model). In this case, vibrations are described by three nonlinear equations. To obtain equations of motion, one can apply Lagrange's equations. After linearization in the inertial co-ordinate system, rotor vibrations are described in the rotating co-ordinates system.

First, the coupling effect and its influence on the stability will be considered in the classical way (Muszyńska *et al.*, 1992). Next, we define the feedback in the coupled system and carry out investigation of the system stability with the help of the Evans method known from the control theory (Takahashi *et al.*, 1972). Such an approach leads to simple explanation when a given intersection on the map of natural frequencies is stable or not.

2. Mathematical model

We consider the physical model of a flexible rotor shown in Fig. 1. The model consists of a rigid disc and a massless flexible shaft. The unbalanced disc is located at the midspan of the shaft. The shaft is driven by a motor which rotates with a constant angular speed Ω. The disc has a mass m and moment of inertia I_o. We assume that the flexibility of the shaft in both directions ξ, η are the same and the stiffness coefficients are $k_1 = k_2 = k$. The torsional flexibility is k_t.

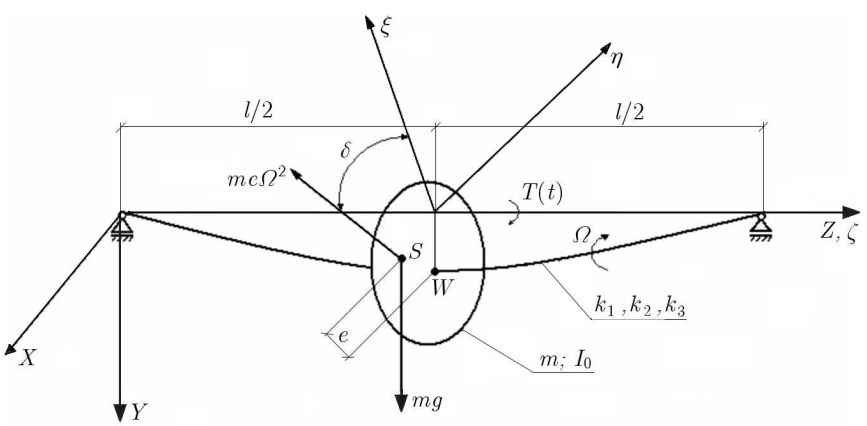

Fig. 1. Physical model of the symmetric rotor

Kinetic E_k and potential E_p energies of such a dynamical system are as follows

$$E_k = \frac{m}{2}(\dot{x}_S^2 + \dot{y}_S^2) + \frac{I_O}{2}\dot{\gamma}^2$$

$$E_p = E_p = \frac{k}{2}\xi^2 + \frac{k}{2}\eta^2 + \frac{k_t}{2}(\gamma - \Omega t)^2 - mgh$$

where

$$x_s = x - e\cos(\gamma+\delta) \qquad y_s = y + e\sin(\gamma+\delta)$$

are coordinates of the disc mass centre S in the inertial coordinate system XYZ, while

$$\xi = x\cos\gamma + y\sin\gamma \qquad \eta = -x\sin\gamma + y\cos\gamma$$

are co-ordinates of the disc geometrical centre W in the rotating co-ordinate system $\xi\eta\zeta$, which rotates with the rotor angular velocity Ω. Furthermore, γ is the angle of the shaft twist, e – the eccentricity (distance) of the rotor mass centre S from its geometrical centre W, while δ is the angle between the unbalance vector and the axis ξ. We omit energy dissipation caused by external and internal damping.

Lagrange's equations were used to obtain the equations of motion of the rotor. They have the form

$$\begin{aligned}
&\ddot{x} - e[\dot{\gamma}^2\cos(\gamma+\delta) + \ddot{\gamma}\sin(\gamma+\delta)] + \omega^2 x = 0\\
&\ddot{y} + e[\ddot{\gamma}\cos(\gamma+\delta) - \dot{\gamma}^2\sin(\gamma+\delta)] + \omega^2 y = 0\\
&\ddot{\gamma} + \mathrm{Re}\ddot{\gamma} + R[\ddot{y}\cos(\gamma+\delta) - \ddot{x}\sin(\gamma+\delta)] + \mu(\gamma - \Omega t) = T(t)
\end{aligned} \tag{2.1}$$

where

$$\omega^2 = \frac{k}{m} \qquad \mu^2 = \frac{k_t}{I_0} \qquad R = \frac{me}{I_0}$$

and $T(t)$ is the difference between the driving and loading torque. It is seen that the equations are nonlinear and coupled by rotor unbalance $(e \neq 0)$.

We introduce coordinates of forward and backward motion

$$u = x + \mathrm{j}y \qquad \overline{u} = x - \mathrm{j}y \tag{2.2}$$

which allows us to represent equation of motion (2.1) in complex inertial co-ordinates as follows

$$\begin{aligned}
&\ddot{u} - e\dot{\gamma}^2\mathrm{e}^{\mathrm{j}(\gamma+\delta)} + \mathrm{j}e\ddot{\gamma}\mathrm{e}^{\mathrm{j}(\gamma+\delta)} + \omega^2 u = \mathrm{j}g\\
&\ddot{\overline{u}} - e\dot{\gamma}^2 e^{-\mathrm{j}(\gamma+\delta)} - \mathrm{j}e\ddot{\gamma}\mathrm{e}^{-\mathrm{j}(\gamma+\delta)} + \omega^2\overline{u} = -\mathrm{j}g\\
&\ddot{\gamma} + \mathrm{Re}\ddot{\gamma} + \frac{R}{2\mathrm{j}}\left[\ddot{u}\mathrm{e}^{-\mathrm{j}(\gamma+\delta)} - \ddot{\overline{u}}\mathrm{e}^{\mathrm{j}(\gamma+\delta)}\right] + \mu^2(\gamma - \Omega t) = T(t)
\end{aligned} \tag{2.3}$$

Equation sets (2.1) and (2.3) are sets of nonlinear and coupled equations.

To start analysis of rotor vibrations, we linearize (2.3) assuming that the torsional difference γ from the angle ΩT by $\phi(t)$

$$\gamma = \Omega t + \phi(t) \tag{2.4}$$

so $\phi(t)$ describes torsional vibrations of the shaft. During linearization, we take into account only first linear components of the Taylor series

$$\mathrm{e}^{\pm \mathrm{j}\phi} = 1 \pm \mathrm{j}\phi + \ldots$$

The linearized set of equations in the inertial complex coordinates has the following form

$$\begin{aligned}
&\ddot{u} + e(-\Omega^2 - \mathrm{j}\Omega^2\phi - 2\Omega\dot{\phi} + \mathrm{j}\ddot{\phi})\mathrm{e}^{\mathrm{j}(\Omega t+\delta)} + \omega^2 u = \mathrm{j}g \\
&\ddot{\overline{u}} + e(-\Omega^2 + \mathrm{j}\Omega^2\phi - 2\Omega\dot{\phi} - \mathrm{j}\ddot{\phi})\mathrm{e}^{-\mathrm{j}(\Omega t+\delta)} + \omega^2\overline{u} = -\mathrm{j}g \\
&\ddot{\phi} + eR\ddot{\phi} + \frac{R}{2\mathrm{j}}\Big[\ddot{u}\mathrm{e}^{-\mathrm{j}(\Omega t+\delta)} - \ddot{\overline{u}}\mathrm{e}^{\mathrm{j}(\Omega t+\delta)}\Big] + \mu^2\phi = T(t)
\end{aligned} \tag{2.5}$$

Now, we introduce the transformation of the coordinates

$$u = w\mathrm{e}^{\mathrm{j}\Omega t} \qquad \overline{u} = \overline{w}\mathrm{e}^{-\mathrm{j}\Omega t} \tag{2.6}$$

where

$$w = \xi + \mathrm{j}n \qquad \overline{w} = \xi - \mathrm{j}n \tag{2.7}$$

which allows us to transfer set (2.5) into a set of rotor dynamical equations in the complex rotating co-ordinates

$$\begin{aligned}
&\ddot{w} + 2\mathrm{j}\Omega\dot{w} - \Omega^2 w + e(\mathrm{j}\ddot{\phi} - 2\Omega\dot{\phi} - \mathrm{j}\Omega^2\phi)\mathrm{e}^{\mathrm{j}\delta} + \omega^2 w = e\Omega^2\mathrm{e}^{\mathrm{j}\delta} + \mathrm{j}g\mathrm{e}^{-\mathrm{j}\Omega t} \\
&\ddot{\overline{w}} - 2\mathrm{j}\Omega\dot{\overline{w}} - \Omega^2\overline{w} + e(-\mathrm{j}\ddot{\phi} - 2\Omega\dot{\phi} - \mathrm{j}\Omega^2\phi)\mathrm{e}^{-\mathrm{j}\delta} + \omega^2\overline{w} = e\Omega^2\mathrm{e}^{-\mathrm{j}\delta} - \mathrm{j}g\mathrm{e}^{\mathrm{j}\Omega t} \\
&\ddot{\phi} + Re\phi + \mu^2\phi + \frac{R}{2\mathrm{j}}\Big[(\ddot{w} + 2\mathrm{j}\Omega\dot{w} - \Omega^2 w)\mathrm{e}^{-\mathrm{j}\delta} - (\ddot{\overline{w}} - 2\mathrm{j}\Omega\dot{\overline{w}} - \Omega^2\overline{w})\mathrm{e}^{\mathrm{j}\delta}\Big] = T(t)
\end{aligned} \tag{2.8}$$

The first two equations are introduced to the third one with the external and internal dampings neglected. By transforming (2.7), we have obtained the equations of motion in real rotating co-ordinates

$$\begin{aligned}
&\ddot{\xi} - 2\Omega\dot{\eta} - \Omega^2\xi + \omega_1^2\xi + e\Omega^2\phi\sin\delta - 2e\Omega\phi\cos\delta - e\phi\sin\delta = \\
&\quad = e\Omega^2\cos\delta + g\sin(\Omega t) \\
&\ddot{\eta} + 2\Omega\dot{\xi} - \Omega^2\eta + \omega_2^2\eta + e\Omega^2\phi\cos\delta - 2e\Omega\phi\sin\delta + e\phi\cos\delta = \\
&\quad = e\Omega^2\sin\delta + g\cos(\Omega t) \\
&\ddot{\phi} + Re\Omega^2\phi + \mu^2\phi + R\omega^2\sin(\delta\xi) - R\omega^2\cos(\delta\eta) = T(t) - Rg\cos(\Omega t + \delta)
\end{aligned} \tag{2.9}$$

Linearized equations in inertial coordinates (2.5) have time dependent coefficients. It means that the rotor vibrations can be considered as parametric vibrations. From the vibration theory we know that such vibrations for some parameters can be unstable. The angular speed Ω is one of the main rotor parameters. Equations in rotating coordinates (2.8) and (2.9) have constant coefficients. Therefore, calculations of unstable ranges of the angular speed will be much simpler by analysing equations (2.9) in the rotating coordinates.

3. Free lateral/torsional vibrations

In this case, equations of motion (2.9) describe free undamped vibrations of the rotor

$$\begin{aligned}
&\ddot{\xi} - 2\Omega\dot{\eta} - \Omega^2\xi + \omega^2\xi + e\Omega^2\phi\sin\delta - 2e\Omega\dot{\phi}\cos\delta - e\ddot{\phi}\sin\delta = 0\\
&\ddot{\eta} + 2\Omega\dot{\xi} - \Omega^2\eta + \omega^2\eta - e\Omega\phi\cos\delta - 2e\Omega\dot{\phi}\sin\delta + e\ddot{\phi}\cos\delta = 0\\
&\ddot{\phi} + eR\Omega^2\phi + \mu^2\phi + R\omega^2\xi\sin\delta - R\omega^2\eta\cos\delta = 0
\end{aligned} \tag{3.1}$$

After application of the Laplace transformation, the differential equations change into the algebraic form as follows

$$\begin{bmatrix} s^2 - \Omega^2 + \omega^2 & -2\Omega s & e\Omega^2\sin\delta - 2e\Omega s\cos\delta - es^2\sin\delta \\ 2\Omega s & s^2 - \Omega^2 + \omega^2 & -e\Omega^2\cos\delta - 2e\Omega s\sin\delta + es^2\cos\delta \\ R\omega^2\sin\delta & -R\omega^2\cos\delta & s^2 + eR\Omega^2 + \mu^2 \end{bmatrix} \begin{bmatrix} \xi \\ \eta \\ \phi \end{bmatrix} = \begin{bmatrix} 0 \\ 0 \\ 0 \end{bmatrix} \tag{3.2}$$

From the above matrix we can obtain the characteristic equation

$$s^6 + a_1 s^4 + a_2 s^2 + a_3 = 0 \tag{3.3}$$

where

$$\begin{aligned}
a_1 &= 2\omega^2 + 2\Omega^2 + \mu_z^2 + pR_h\\
a_2 &= (\omega^2 - \Omega^2)^2 + 2(\omega^2 + \Omega^2)\mu_z^2 + \omega^4 R_h + 2\Omega^2 pR_h\\
a_3 &= \mu_z^2(\omega^2 - \Omega^2)^2 - \omega^4 R_h + \Omega^4 pR_h\\
p &= \omega^2 \qquad R_h = Re = \frac{me^2}{I_0} \qquad \mu_z^2 = \mu^2 + R_h\Omega^2
\end{aligned}$$

In the above formulas for coefficients of the characteristic equation the parameter δ, angle between the unbalance vector and the axis ξ, does not

influence the roots. This is only true in the case of an isotropic rotor. Therefore, we can orient the rotating coordinate system in any way with respect to the rotor. It can be seen from the last equation that the unbalance influences the natural frequency of torsional vibration. This influence is shown in Fig. 2.

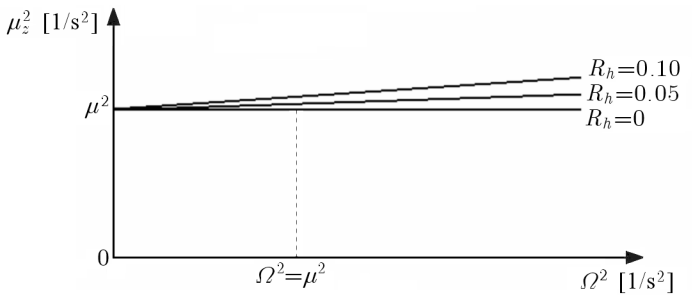

Fig. 2. Effect of non-dimensional unbalance on the torsional natural frequency

For small values of the unbalance it can be assumed (see Fig. 2) that $\mu_z \equiv \mu \equiv= \text{const}$.

The system is stable when all roots of the characteristic equation have negative real parts. Using the Cardan solution of the 3-order for algebraic equation (3.3), we have obtained the stability conditions

$$a_3 > 0 \qquad a_1 > 0 \tag{3.4}$$

and

$$a_1^2 < 3a_2 \qquad \text{or} \qquad 2(a_1^2 - 3a_2)^3 > [a_l(9a_2 - 2a_1^2) - 27a_3]^2$$

when $a_1^2 > 3a_2$.

From first inequality (3.4), we can calculate one of the unstable ranges of the rotor speed

$$\omega\sqrt{\frac{\mu_z^2}{R_h\omega^2 + \mu_z^2}} < \Omega < \omega \tag{3.5}$$

It is seen that the unstable range always exists when the rotor is unbalanced ($e \neq 0$).

Second inequality (3.4) is always satisfied. From third inequality (3.4) we can extract one more range of the unstable rotor speed. The range is in the vicinity of the value

$$\Omega = \omega + \mu \tag{3.6}$$

The analytical considerations are confirmed by the computer simulation results. The changes of natural frequencies as a function of rotor angular speed

are shown in Figs. 3-5. In all simulations we have obtain both mentioned ranges of unstable rotor speeds.

Because of symmetry, in Figs. 3-5 and further figures, we show only one quarter of the calculated natural frequencies. The unstable speeds are at the vicinity of intersection of natural frequencies. For these frequencies, the real part of roots has positive values (see plots (a) in mentioned Figs. 3-5). We denote by p_i the ith pole of the transfer function (root of the characteristic polynomial) and by z_i the ith zero of transfer function.

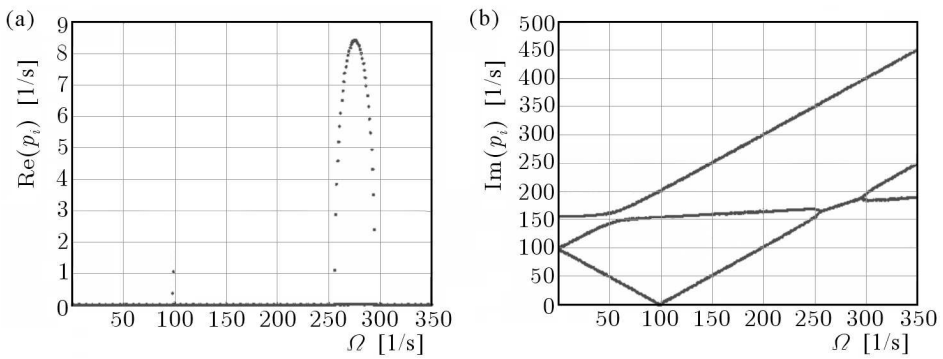

Fig. 3. Real (a) and imaginary (b) parts of characteristic polynomial roots versus rotor speed Ω for: $\omega = 100\,\mathrm{s}^{-1}$, $\mu = 150\,\mathrm{s}^{-1}$, $R_h = 0.1$. Two ranges of unstable rotor speed: $97\,\mathrm{s}^{-1} < \Omega < 100\,\mathrm{s}^{-1}$, $256\,\mathrm{s}^{-1} < \Omega < 292\,\mathrm{s}^{-1}$

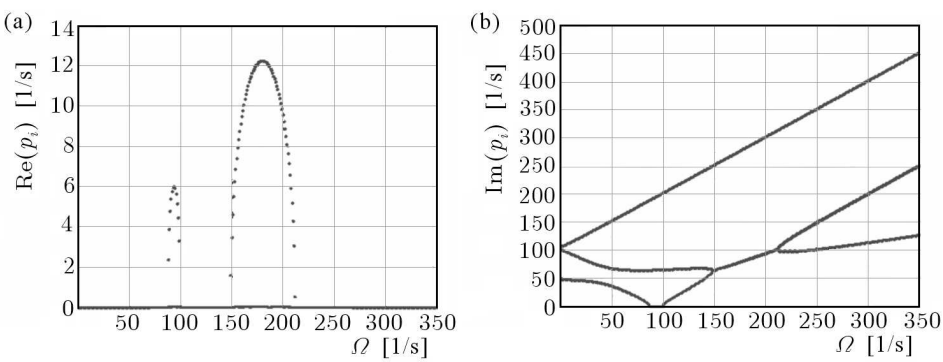

Fig. 4. Real (a) and imaginary (b) parts of characteristic polynomial roots versus rotor speed Ω for: $\omega = 100\,\mathrm{s}^{-1}$, $\mu = 50\,\mathrm{s}^{-1}$, $R_h = 0.1$. Two ranges of unstable rotor speed: $81\,\mathrm{s}^{-1} < \Omega < 100\,\mathrm{s}^{-1}$, $148\,\mathrm{s}^{-1} < \Omega < 213\,\mathrm{s}^{-1}$

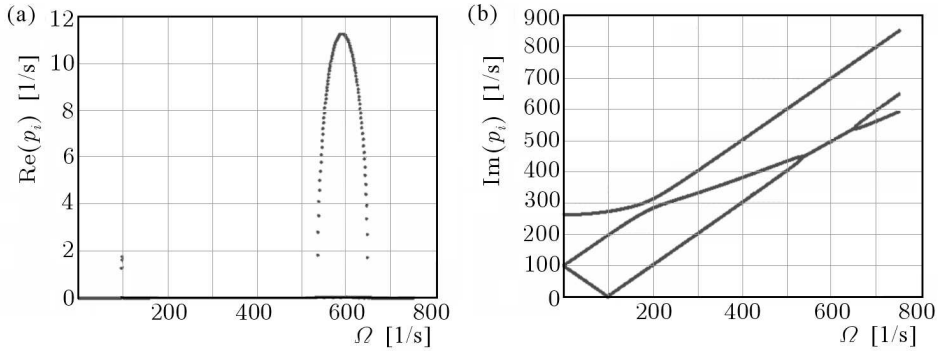

Fig. 5. Real (a) and imaginary (b) parts of characteristic polynomial roots versus rotor speed Ω for: $\omega = 100\,\mathrm{s}^{-1}$, $\mu = 250\,\mathrm{s}^{-1}$, $R_h = 0.1$. Two ranges of unstable rotor speed: $96\,\mathrm{s}^{-1} < \Omega < 100\,\mathrm{s}^{-1}$, $545\,\mathrm{s}^{-1} < \Omega < 664\,\mathrm{s}^{-1}$

4. Coupling of torsional/lateral vibrations as a feedback loop

In the above analysis we have found that the unstable ranges of the rotor speed appear in the vicinity of some angular speeds for which the lines of natural frequencies intersect with each other. But not all the intersections are the cause of unstable behaviour of free vibrations. So, the problem arises how to recognize which of the crossings indicates the unstable ranges. To answer this question, we reach for synthesis methods known from the theory of control.

We repeat equation (3.2) in a compact form

$$\begin{bmatrix} A(s) & -B(s) & -D(s) \\ B(s) & A(s) & -F(s) \\ -K(s) & -H(s) & C(s) \end{bmatrix} \begin{bmatrix} \xi \\ \eta \\ \phi \end{bmatrix} = 0 \tag{4.1}$$

where

$$A(s) = s^2 - \Omega^2 + \omega^2 \qquad B(s) = 2\Omega s$$

$$C(s) = s^2 + eR\Omega^2 + \mu^2 \qquad D(s) = -e(\Omega^2 \sin\delta - 2\Omega s\cos\delta - s^2\sin\delta)$$

$$H(s) = -R\omega_2^2 \sin\delta \qquad F(s) = e(\Omega^2\cos\delta + 2\Omega s\sin\delta - s^2\cos\delta)$$

$$K(s) = R\omega_1^2\cos\delta$$

We consider now separately lateral and torsional vibrations. The coupling forces are assumed as external excitations

$$A(s)\xi(s) - B(s)\eta(s) = D(s)\varphi(s) \qquad B(s)\xi(s) + A(s)\eta(s) = F(s)\varphi(s)$$

$$C(s)\varphi(s) = H(s)\xi(s) + K(s)\eta(s) \tag{4.2}$$

The first two equations describe lateral vibrations while the third one describes torsional vibrations. The mathematical model can be presented in the form of a block diagram, given in Fig. 6.

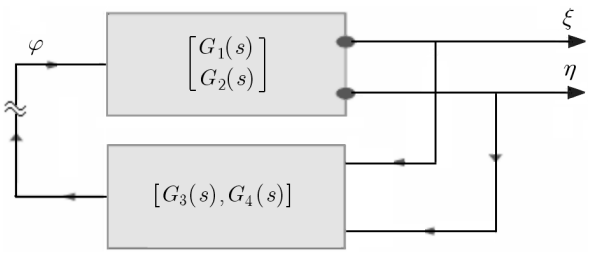

Fig. 6. Block scheme of torsional/lateral vibrations of the flexible rotor

It is a dynamical system with a feedback loop very well known from theory of control, where particular transfer functions have the form

$$\begin{aligned} G_1(s) &= \frac{\xi(s)}{\varphi(s)} = \frac{B(s)F(s) + A(s)D(s)}{A^2(s) + B^2(s)} \\ G_2(s) &= \frac{\eta(s)}{\varphi(s)} = \frac{A(s)F(s) - B(s)D(s)}{A^2(s) + B^2(s)} \\ G_3(s) &= \frac{\varphi(s)}{\xi(s)} = \frac{H(s)}{C(s)} \qquad G_4(s) = \frac{\varphi(s)}{\eta(s)} = \frac{K(s)}{C(s)} \end{aligned} \tag{4.3}$$

We break the feedback loop in the place indicated by tildes to obtain an open-loop system. The open-loop transfer function is obtained by multiplication of the matrices

$$G_o(s) = [G_3(s), G_4(s)] \begin{bmatrix} G_1(s) \\ G_2(s) \end{bmatrix} = G_3(s)G_1(s) + G_4(s)G_2(s) \tag{4.4}$$

Taking into account transfer functions (4.3), we have

$$G_o(s) = \frac{H(s)B(s)F(s) + H(s)A(s)D(s) + K(s)A(s)F(s) - K(s)B(s)D(s)}{[A^2(s) + B^2(s)]C(s)}$$

When we introduce rotor parameters (4.1), the open loop transfer function has the form

$$G_o(s) = \frac{-R_h\omega^2[s^4 + s^2(2\Omega^2 + \omega^2) - (\omega^2 - \Omega^2)\Omega^2]}{[s^4 + s^2 2(\omega^2 + \Omega^2) + (\omega^2 - \Omega^2)](s^2 + \mu_z^2)} = R_h G_r(s) \tag{4.5}$$

In the Evans method, we consider the rotor unbalance parameter R_h as a gain which varies from zero to infinity.

5. Evans method

Now we analyse the influence of the unbalance on the system dynamics. The closed loop system from Fig. 6 have the following characteristic equation

$$1 + R_h G_r(s) = 0 \qquad \text{or} \qquad G_r(s) = -\frac{1}{R_h} \qquad \text{for} \quad R_h \geqslant 0 \tag{5.1}$$

In our case, the characteristic equation of the closed-loop system has the form

$$1 + \frac{-R_h\omega^2[s^4 + s^2(2\Omega^2 + \omega^2) - (\omega^2 - \Omega^2)\Omega^2]}{[s^4 + s^2 2(\omega^2 + \Omega^2) + (\omega^2 - \Omega^2)](s^2 + \mu_z^2)} = 0$$

or

$$\frac{1}{[s^4 + s^2 2(\omega^2 + \Omega^2) + (\omega^2 - \Omega^2)](s^2 + \mu_z^2)} \Big\{ [s^4 + s^2 2(\omega^2 + \Omega^2) + (\omega^2 - \Omega^2)] \cdot \tag{5.2}$$

$$\cdot (s^2 + \mu_z^2) - R_h\omega^2[s^4 + s^2(2\Omega^2 + \omega^2) - (\omega^2 - \Omega^2)\Omega^2] \Big\} = 0$$

We can simply check that the numerator of transfer function (5.2) is a characteristic polynomial of closed-loop system (5.2), and the denominator is a characteristic polynomial of the open-loop system.

$G_r(s)$ is a complex number and can be represented by a vector on the complex plane. So, according to equation (5.1), the transfer function $G_r(s)$ should satisfy two conditions imposed on the angular location of the vector

$$\arg G_r(s) = -180^\circ \pm 360^\circ N \tag{5.3}$$

where N – integer number and on its absolute value

$$|G_r(s)| = \frac{1}{R_h} \tag{5.4}$$

From the above conditions one can conclude that for R_h increasing from zero to infinity, the open-loop poles (roots of the numerator polynomial in the transfer function $G_r(s)$) move towards zeros of the same open-loop transfer function $G_r(s)$ (roots of the nominator in equation (4.6)). If the number of poles is bigger than the number of zeros, other poles escape to infinity along asymptotes which start from the central point on the complex plane.

It means that zeros of the open-loop transfer function should play an important role in the analysis of the unbalance effect on dynamical behaviour of coupled torsional/lateral vibrations of the flexible rotor. The real and imaginary parts of the transfer function zeros for the rotor parameters: $\omega = 100\,\mathrm{s}^{-1}$,

$\mu = 150\,\mathrm{s}^{-1}$, $R_h = 0.1$ are presented in Fig. 7. It is a rotor, whose poles (natural frequencies) are given in Fig. 3. Two ranges of unstable rotor speeds are: $97\,\mathrm{s}^{-1} < \Omega < 100\,\mathrm{s}^{-1}$ and $256\,\mathrm{s}^{-1} < \Omega < 292\,\mathrm{s}^{-1}$. From now, all calculations will be carried out for this case.

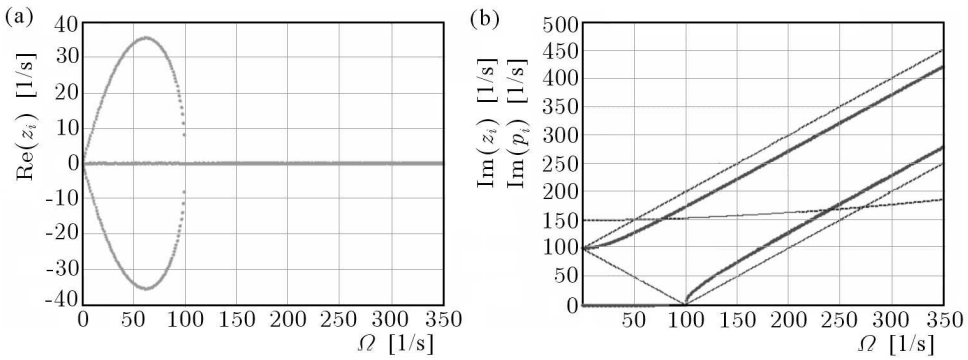

Fig. 7. Real (a) and imaginary (b) parts of zeros in the transfer function $G_r(s)$ versus rotor angular speed Ω drown as bold lines. Slim lines in (b) show natural frequencies of uncoupled torsional/lateral vibrations (poles of the transfer function $G_r(s)$

As we can see in Fig. 7, the nonzero (positive and negative) real parts of the zeros exist only for the rotor speed Ω ranging from $0\,\mathrm{s}^{-1}$ to $100\,\mathrm{s}^{-1}$. Imaginary parts (frequencies) of the zeros change together with the rotor angular speed Ω and increase parallel to real parts of the poles (natural frequencies) of the lateral vibrations.

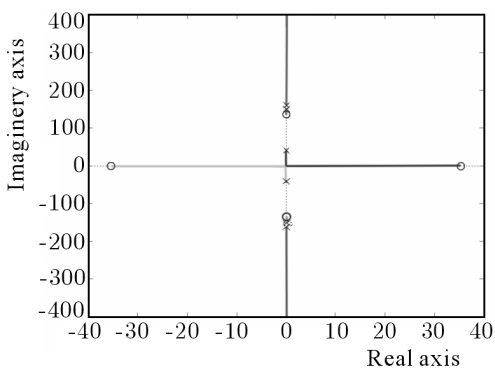

Fig. 8. Root locus of unbalanced torsional/lateral vibrations for rotor angular speed $60\,\mathrm{s}^{-1}$ when the unbalance R_h changes from 0 to infinity

For a smaller angular speed of the rotor ($60\,\mathrm{s}^{-1}$ in Fig. 8), the system can be unstable for very big values of R_h because two of the zeros in the transfer

function $G_r(s)$ are real and positive. But the value of unbalance for which it works is unrealistic.

The root locus for the first range of unstable speed ($99\,\mathrm{s}^{-1}$) is shown in Fig. 9. It is seen that for small unbalances ($R_h > 0.045$), motion of the rotor becomes unstable because of the positive zeros in the transfer function.

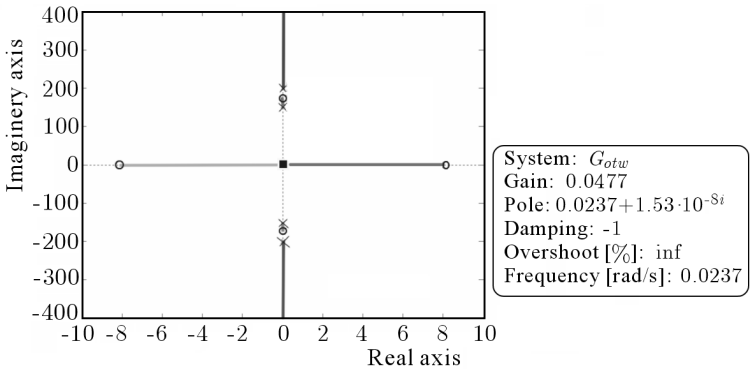

Fig. 9. Root locus of unbalanced torsional/lateral vibrations for rotor angular speed $99\,\mathrm{s}^{-1}$ when the unbalance R_h changes from 0 to infinity

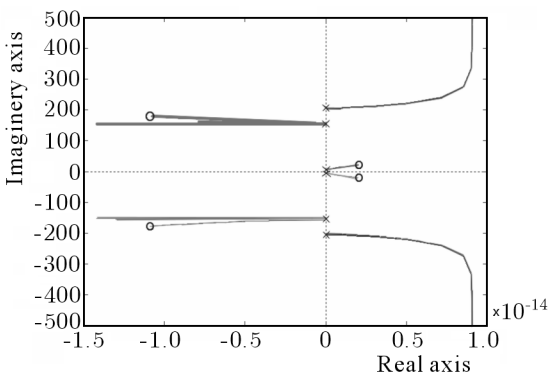

Fig. 10. Root locus of unbalanced torsional/lateral vibrations for rotor angular speed $105\,\mathrm{s}^{-1}$ when the unbalance R_h changes from 0 to infinity. All poles, zeros and root locus lines lie on the imaginary axis. The 10^{-14}-order shift of the zeros and poles from the imaginary axis is caused by numerical errors

When all zeros and poles of the transfer function are purely imaginary, plot of the the root locus shows their location with well seen errors. They are very small computation errors. In this case the poles move along the imaginary axis. In this case, each pole has its associated zero which is a target for the locus line. Two biggest poles move to infinity along the imaginary axis. Such a rotor is completely stable for all values of the unbalance R_h.

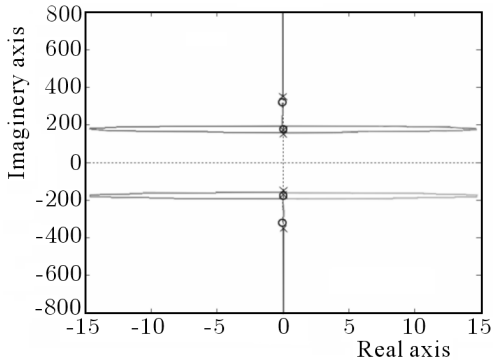

Fig. 11. Root locus of unbalanced torsional/lateral vibrations for rotor angular speed $250\,\mathrm{s}^{-1}$ when the unbalance R_h changes from 0 to infinity

Such harmony is destroyed when the rotor angular speed crosses $245\,\mathrm{s}^{-1}$ (see Fig. 11). For angular speed $\Omega = 250\,\mathrm{s}^{-1}$, the alteration of poles and zeros is replaced by close neighbourhood of two poles. To reach the zeros, the locus lines are forced to make circles. The circles enter the positive side of the complex plane. It means that motion becomes unstable for some values of the unbalance. On a magnified picture (Fig. 12), the gain $R_h > 0.21$ for the rotor speed $\Omega = 250\,\mathrm{s}^{-1}$ is sufficient to destabilize motion. The dynamic behaviour of the rotor is similar for $\Omega = 270\,\mathrm{s}^{-1}$ (Figs. 13 and 14) but motion becomes unstable for much smaller value of the unbalance ($R_h > 0.001$) than in the case of the rotor speed $\Omega = 250\,\mathrm{s}^{-1}$.

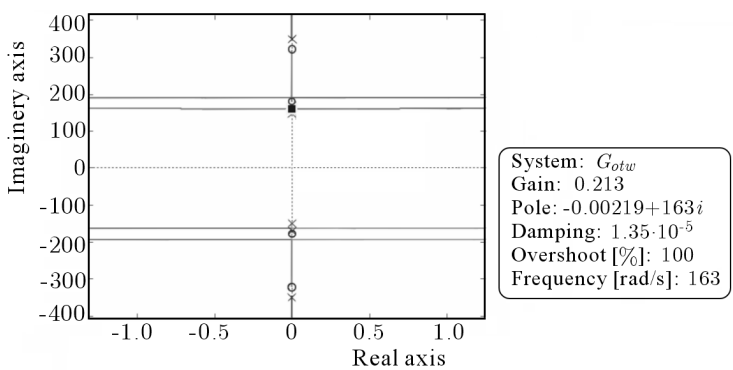

Fig. 12. Root locus of the system for rotor angular speed $250\,\mathrm{s}^{-1}$. A magnified part of interest of Fig. 11

For higher angular speeds of the rotor, we have the same dynamical behaviour of the rotor but the unstable motion is excited by bigger values of unbalance (see Figs. 15 and 16).

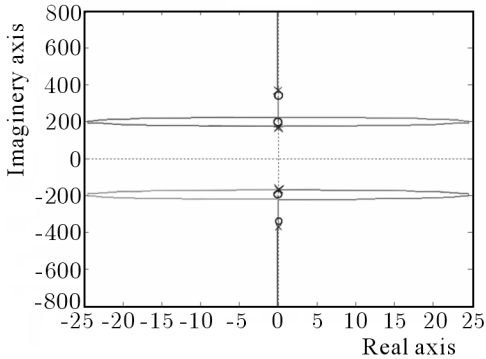

Fig. 13. Root locus of unbalanced torsional/lateral vibrations for rotor angular speed $270\,\mathrm{s}^{-1}$ when the unbalance R_h changes from 0 to infinity

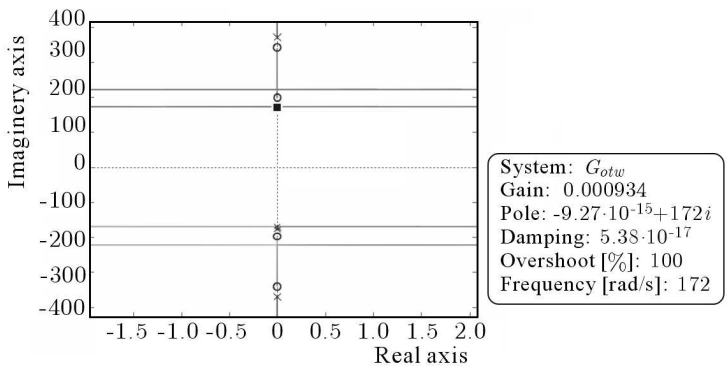

Fig. 14. Root locus of the system for rotor angular speed $270\,\mathrm{s}^{-1}$. A magnified part of interest of Fig. 13

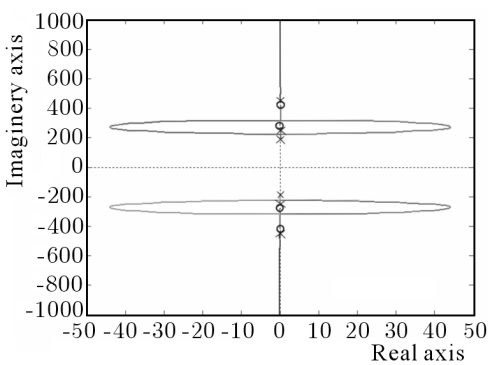

Fig. 15. Root locus of the system for rotor angular speed $350\,\mathrm{s}^{-1}$

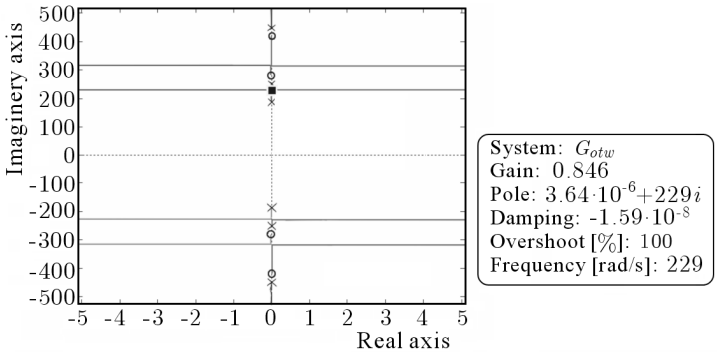

Fig. 16. 16. Root locus of the system for rotor angular speed $350\,\mathrm{s}^{-1}$. A magnified part of interest of Fig. 15

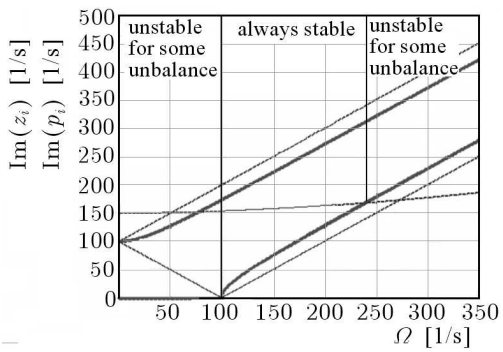

Fig. 17. Ranges of the rotor speed with unbalances which can destabilize rotor vibrations

After all considerations, we conclude that we are able to show the ranges of unstable vibrations (Fig. 17). In the first range (up to $100\,\mathrm{s}^{-1}$), unstable torsional/lateral vibrations are connected with positive value of one zero of the open-loop transfer function. In the second range of ustable rotor angular speeds, the alternating pole-zero pattern is destroyed (Preumont, 2002). The neighbourhood of two zeros or two poles is a simple indicator for detecting unstable behaviour of the system. The closer to the crossing point the smaller value of the unbalance is needed to trigger the instability in both ranges.

6. Conclusions

The theory of control tools has been employed in the analysis of coupled vibrations of the rotor. Using Evans' method, the unstable regions of vibrations

for both coupled systems have been demonstrated. Analysis of pole and zero locations over a wide range of the rotor angular speed provides complete insight into the rotor dynamics. The generated results can be applied for diagnosing the technical state of rotors and also can be used in the control of rotor vibrations.

References

1. Gosiewski Z., Muszyńska A., 1992, *Dynamika maszyn wirnikowych* (Dynamics of rotating machinery), Publishing Office of WSInż. Koszalin
2. Muszyńska A., Goldman P., Bently D.E., 1992, Torsional/lateral vibration cross-coupled responses due to shaft anisotropy: a new tool in shaft crack detection, *Conference of Institution of Mechanical Engineers*, Bath, Great Britain
3. Sawicki J.T., Baaklini G.Y., Gyekenyesi A.L., 2004, Dynamic analysis of accelerating cracked flexible rotor, *Paper GT2004-54095, Turbo ASME Turbo Expo Conference*, 14-17 June, Vienna, Austria
4. Takahashi Y., Rabbins M.J., Auslander D.M., 1972, *Control and Dynamic Systems*, Addison-Wesley, Reading, MA.
5. Preumout G., 2002, *Vibration Control of Active Structures: An Introduction*, Kluwer Academic Publishers, Dordrecht

Analiza mechanizmu sprzęgającego drgania giętno-skrętne wirnika

Streszczenie

Zjawisko sprzęgania się drgań giętnych i skrętnych w maszynach wirnikowych może prowadzić do niestabilnego ruchu wirnika. W niektórych maszynach wirnikowych prędkość obrotowa wirnika zmienia się w szerokim zakresie. Zadaniem jest znalezienie takich zakresów prędkości obrotowej, dla których ruch wirnika pozostaje stabilny mimo sprzęgania się jego postaci drgań. Zwykle niestabilne zakresy występują w otoczeniu prędkości kątowych, w których przecinają się mapy częstości własnych wyznaczonych oddzielnie dla drgań giętnych i drgań skrętnych. W artykule wykorzystano metodę linii pierwiastkowych, aby wykazać, które przecięcia są niestabilne i dlaczego.

Manuscript received March 19, 2008; accepted for print May 19, 2008